Chapter 11
Crossing Points in Spectra and Light Absorption in Spheroidal and Cone-Shaped Quantum Dots

V. L. Derbov [ORCID]**, A. A. Gusev** [ORCID]**, O. Chuluunbaatar** [ORCID]**, L. L. Hai,**
S. I. Vinitsky [ORCID]**, E. M. Kazaryan, and H. A. Sarkisyan** [ORCID]

Abstract We briefly review the analysis of the energy spectrum, the envelope eigenfunctions of electron, hole and exciton states, and the direct interband light absorption in cone-shaped and spheroidal impenetrable quantum dots. We apply high-order finite element method and calculation schemes of Kantorovich method in comparison with the adiabatic approximation (in the strong size quantization limit) for solving boundary-value problems that describe axially symmetric quantum dots. We demonstrate the efficiency of the algorithms and software by benchmark calculations of spectral and optical characteristics of the cone-shaped and spheroidal quantum dots and crossing points in their spectra.

V. L. Derbov
N.G. Chernyshevsky Saratov National Research State University, Saratov, Russia

A. A. Gusev (✉) · O. Chuluunbaatar · S. I. Vinitsky
Joint Institute for Nuclear Research, Dubna, MR 141980, Russia
e-mail: gooseff@jinr.ru

O. Chuluunbaatar
Institute of Mathematics and Digital Technology, Mongolian Academy of Sciences, Ulaanbaatar 13330, Mongolia

L. L. Hai
Ho Chi Minh city University of Education, Ho Chi Minh city, Vietnam

S. I. Vinitsky
Peoples' Friendship University of Russia (RUDN University), 117198 Moscow, Russia

E. M. Kazaryan · H. A. Sarkisyan
Russian-Armenian (Slavonic) University, H. Emin 123, 0051 Yerevan, Armenia

H. A. Sarkisyan
Peter the Great Saint-Petersburg Polytechnic University, Polytechnicheskaya 29, St. Petersburg 195251, Russia

129

11.1 Introduction

The study of spectral and optical characteristics of quantum wells, wires and dots with complicated geometry is an urgent problem of both computational and theoretical physics. To solve boundary-value problems (BPVs) that describe corresponding mathematical models, they commonly use finite-difference and variational methods [1], finite element method (FEM) [2–7], Kantorovich method (KM)-reduction to ordinary differential equations(ODEs) [8–14], known in physics as adiabatic method [15], and adapted in the field [16–21].

In this paper, we present a brief review of application of high-order FEM calculation schemes implemented on unstructured grids with triangle elements [4, 5] and KM for solving the BVPs that describe spectral and optical characteristics of cone-shaped and spheroidal quantum dots and crossing points in their spectra *to obtain independent estimates of the applicability range and accuracy of conventional adiabatic approximation (AA) (in the strong size quantization limit), i.e., a diagonal set of the KM-ODEs developed early by our team.* We discuss the application of these methods and appropriate software to the calculation of the energy spectra of electron, hole and exciton states the direct interband light absorption and the light absorption coefficient in ensembles of non-interacting cone-shaped and spheroidal impenetrable quantum dots (QDs).

The paper is organized as follows. In Sect. 11.2 we set the boundary value problem. Section 11.3 presents the basis equations of the Kantorovich method. In Sect. 11.4 we describe the numerical calculations of the energy spectrum of the QDs. Section 11.5 is devoted to the adiabatic approximation. In Sect. 11.6 we give examples of the interband absorption in QDs. In Conclusions we resume the results and discuss the prospects.

11.2 Setting the Problem

Within the effective mass approximation we consider a class of QD models in which the calculation of energy levels and corresponding envelope eigenfunctions is reduced to self-adjoint BVPs for elliptic differential equations [2]

$$(H - \mathcal{E}_t)\,\Psi_t(x) \equiv \left(-\frac{1}{g_0(x)} \sum_{ij=1}^{d} \frac{\partial}{\partial x_i} g_{ij}(x) \frac{\partial}{\partial x_j} + V(x) - \mathcal{E}_t \right) \Psi_t(x) = 0. \quad (11.1)$$

We assume that $g_0(x) > 0$, $g_{ji}(x) = g_{ij}(x)$ and $V(x)$ are real-valued functions, continuous together with their generalized derivatives to a given order in the domain $x \in \bar{\Omega} = \Omega \cup \partial\Omega$ with the piecewise continuous boundary $S = \partial\Omega$, which provides the existence of a nontrivial solution obeying the mixed boundary conditions (BCs) of the first (I) and/or the second kind (II), i.e., Dirichlet and/or Neumann conditions:

$$(I)\ \Psi_t(x)|_S = 0,\ (II)\ \frac{\partial \Psi(x)}{\partial n_D}\bigg|_S = 0,\ \ \frac{\partial \Psi_t(x)}{\partial n_D} = \sum_{ij=1}^{d}(\hat{n}, \hat{e}_i)g_{ij}(x)\frac{\partial \Psi_t(x)}{\partial z_j}, \quad (11.2)$$

where $\frac{\partial \Psi_t(x)}{\partial n_D}$ is the derivative along the conormal direction, $\hat{n}$ is the outer normal to the boundary of the domain $S = \partial\Omega$, $\hat{e}_i$ is the unit vector of $x = \sum_{i=1}^{d}\hat{e}_i x_i$, and $(\hat{n}, \hat{e}_i)$ is the scalar product in $\mathcal{R}^d$. The eigenfunctions $\Psi_t(x)$ from the Sobolev space $\mathcal{H}_2^{s\geq 1}(\Omega)$, $\Psi_t(x) \in \mathcal{H}_2^{s\geq 1}(\Omega)$, corresponding to the real eigenvalues of energy spectrum $\mathcal{E}:\mathcal{E}_1\leq\mathcal{E}_2\leq\ldots\leq\mathcal{E}_t\leq\ldots$ satisfy the orthonormality conditions

$$\langle \Psi_t(x)|\Psi_{t'}(x)\rangle = \int_\Omega dx g_0(x)\Psi_t(x)\Psi_{t'}(x) = \delta_{tt'}, \quad dx = dx_1...dx_d. \quad (11.3)$$

We solve this problem using high-accuracy finite element schemes, implemented in the appropriate algorithms and programs [4, 5].

11.3   Kantorovich Method

The axially symmetric solutions of the BVP (11.1)–(11.3) at $d = 3$, periodical with respect to the azimuthal angle φ, are sought in the form of a product $\Psi_t(x_f, x_s, \varphi) = \Psi_t^{m\sigma}(x_f, x_s)e^{im\varphi}/\sqrt{2\pi}$, where $m = 0, \pm 1, \pm 2, \ldots$ is the magnetic quantum number and divided into even ($\sigma = +1$) and odd ($\sigma = -1$) reflection parity ones, or marked $\sigma = 0$, i.e., without parity separation. The function $\Psi_t^{m\sigma}(x_f, x_s)$ is solution of the BVP (11.1)–(11.3) at $d = 2$ and satisfies the equation in the 2D domain Ω: $\Omega = \Omega_{x_f}(x_s)\cup\Omega_{x_s}\subset\mathbf{R}^2\backslash\{0\}$, $\Omega_{x_f}(x_s) = (x_f^{\min}(x_s), x_f^{\max}(x_s))$, $\Omega_{x_s} = (x_s^{\min}, x_s^{\max})$:
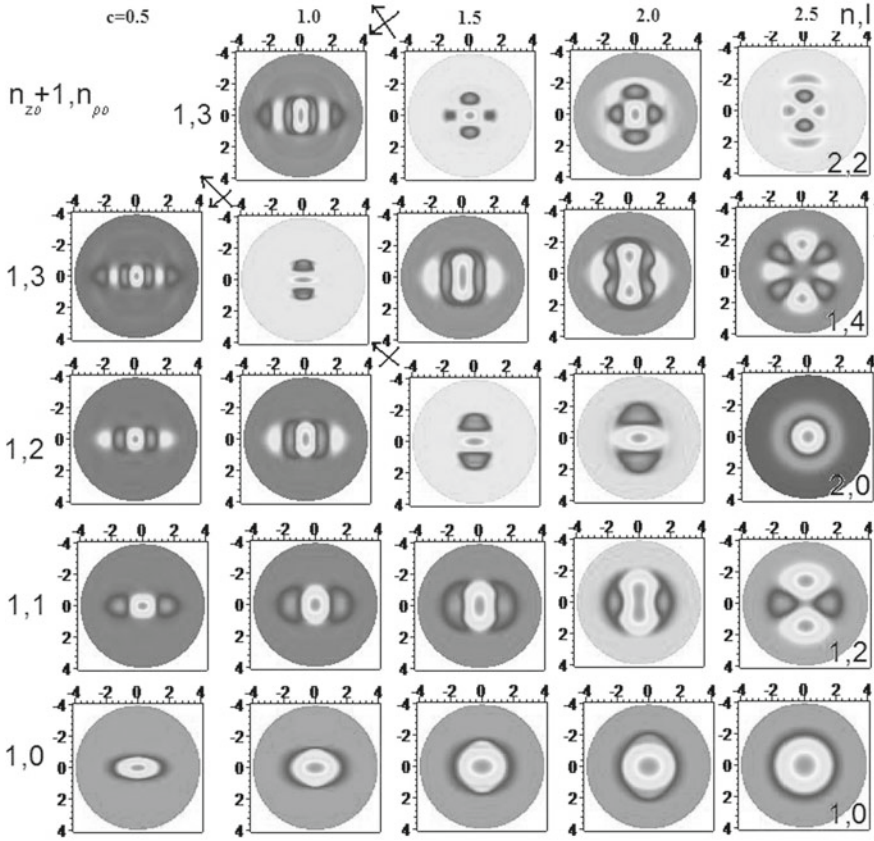
$$\left(\hat{H}(x_f, x_s)-2E_t\right)\Psi_t^{m\sigma}(x_f, x_s) = 0,\ \ \hat{H}(x_f, x_s) = \hat{H}_1(x_f; x_s)+\hat{H}_2(x_f; x_s). \quad (11.4)$$

The Hamiltonian of the slow subsystem $\hat{H}_2(x_f; x_s)$ is expressed as

$$\hat{H}_2(x_f; x_s) = \check{H}_2(x_f; x_s) = -\frac{1}{g_{1s}(x_f; x_s)}\frac{\partial}{\partial x_s}g_{2s}(x_s)\frac{\partial}{\partial x_s} + \check{V}_s(x_f; x_s), \quad (11.5)$$

and the Hamiltonian of the fast subsystem $\hat{H}_1(x_f; x_s)$ is expressed through the reduced Hamiltonian $\check{H}_f(x_f; x_s)$ and the weighting factor $g_{3s}(x_f; x_s)$:

$$\hat{H}_1(x_f; x_s) = g_{3s}^{-1}(x_f; x_s)\check{H}_f(x_f; x_s), \quad (11.6)$$

$$\check{H}_f(x_f; x_s) = -\frac{1}{g_{1f}(x_f)}\frac{\partial}{\partial x_f}g_{2f}(x_f)\frac{\partial}{\partial x_f}+\check{V}_f(x_f)+\check{V}_{fs}(x_f; x_s).$$

Fig. 11.1 Contour lines of the first five even-parity wave functions $\sigma = +1$ at $m = 0$ in the xz plane of an oblate SQD with the major semiaxis $a = 2.5$ and different values of the minor semiaxis c ($\zeta_{ca} = c/a \in (1/5, 1)$). Arrows indicate the shape transformations of the eigenfunctions when passing through the exact crossing points of pairs of eigenvalues

The choice of fast variable x_f (or slow variable x_s), as well as the interaction potentials, is determined by the QD geometry and construction. The separation of Hamiltonian (11.4) into two Hamiltonians (11.5) and (11.6) with partial derivatives with respect to independent slow variable x_s and fast variable x_f is possible, when one of the QD dimensions is small compared to the other ones. Then the size quantization in the direction x_f (x_s) turns to be much stronger (weaker) compared to that in other directions. This feature allows using adiabatic or diagonal Kantorovich approximation in the strong size quantization limit to estimate the lower-energy part of the QD spectrum. Note, for a convergence of the KM it is sufficient if the Hamiltonian of the fast subsystem has a pure discrete spectrum, while an appropriate choice of the fast and slow variables and parametric basis provides a more high rate of the convergence.

Table 11.1 The values of conditionally fast x_f and slow x_s independent variables, coefficients $g_{is}(x_f; x_s)$, $g_{jf}(x_f)$, and potentials $\check{V}_f(x_f)$, $\check{V}_s(x_f; x_s)$, $\check{V}_{fs}(x_f, x_s)$, in Eqs. (11.4)–(11.6) for OCQD and PCQD, or SQD, OSQD and PSQD in cylindrical (CC) and spherical (SC) coordinates, and oblate & prolate spheroidal (OSC & PSC) coordinates with $(f/2)^2 = \pm(a^2 - c^2)$, + for OSC, − for PSC, f is a focal distance, a and c are semiaxes

	CC		SC	OSC & PSC
	OCQD/OSQD	PCQD/PSQD	SQD	OSQD & PSQD
x_f	z	ρ	η	η
x_s	ρ	z	r	ξ
$g_0(x_f; x_s)$	ρ	ρ	r^2	$(f/2)(\xi^2 \pm \eta^2)$
$g_{1f}(x_f)$	1	ρ	1	1
$g_{2f}(x_f)$	1	ρ	$1 - \eta^2$	$1 - \eta^2$
$g_{1s}(x_f\ x_s)$	ρ	1	r^2	g_0
$g_{2s}(x_s)$	ρ	1	r^2	$\xi^2 \pm 1$
$g_{3s}(x_f\ x_s)$	1	1	r^2	g_0
$\check{V}_f(x_f)$	0	$m^2\rho^2$	$m^2 g_{2f}$	$m^2 g_{2f}$
$\check{V}_s(x_f\ x_s)$	$m^2\rho^2$	0	0	$\mp m^2(g_0 g_{2s})$
$\check{V}_{fs}(x_f, x_s)$	$\check{V}(z, \rho)$	$\check{V}(\rho, z)$	$\check{V}(r, \eta)$	$\check{V}(\xi, \eta)$

Table 11.1 contains the values of conditionally fast x_f and slow x_s independent variables, the coefficients $g_0(x_f; x_s)$, $g_{1s}(x_f; x_s)$, $g_{2s}(x_s)$, $g_{3s}(x_f; x_s)$, $g_{1f}(x_f)$, $g_{2f}(x_f)$, and the reduced potentials $\check{V}_f(x_f)$, $\check{V}_s(x_f; x_s)$, $\check{V}_{fs}(x_f, x_s)$, entering Eqs. (11.4)–(11.6) for QDs: spherical SQD, oblate and prolate spheroidal OSQD and PSQD or cone-shaped OCQD and PCQD in cylindrical coordinates (CC) ($\mathbf{x} = (z, \rho, \varphi)$), spherical coordinates (SC) ($\mathbf{x} = (r, \eta = \cos\theta, \varphi)$), and oblate/prolate spheroidal ($\mathbf{x} = (\xi, \eta, \varphi)$) coordinates [22].

In Table 11.1 for the considered QDs with impenetrable walls the potentials $\check{V}_{fs} = 0$ are zero, since the potential is reformulated below in the form of BCs with respect to the variables x_f and x_s. The solution $\Psi_t^{m\sigma}(x_f, x_s)$ of the problem (11.4)–(11.6) is sought in the form of KM expansion [17]

$$\Psi_t^{m\sigma}(x_f, x_s) = \sum_{j=1}^{j_{\max}} \Phi_j^{m\sigma}(x_f; x_s)\chi_j^{(m\sigma t)}(x_s), \qquad (11.7)$$

using as a set of trial functions the eigenfunctions $\Phi_j^{m\sigma}(x_f; x_s)$ of the Hamiltonian $\check{H}_f(x_f; x_s)$ from (11.6), i.e., the solutions of the parametric BVP

$$\left\{\check{H}_f(x_f; x_s) - \check{\lambda}_i(x_s)\right\} \Phi_i^{m\sigma}(x_f; x_s) = 0, \qquad (11.8)$$

in the interval $x_f \in \Omega_{x_f}(x_s)$ depending on the conditionally slow variable $x_s \in \Omega_{x_s}$ as a parameter. These solutions obey the boundary conditions

$$\lim_{x_f \to x_f^t(x_s)} \left(N_f^{(m\sigma)}(x_s) g_{2f}(x_f) \frac{d\Phi_j^{m\sigma}(x_f; x_s)}{dx_f} + D_f^{(m\sigma)}(x_s) \Phi_j^{m\sigma}(x_f; x_s) \right) = 0 \quad (11.9)$$

at the boundary points $\{x_f^{\min}(x_s), x_f^{\max}(x_s)\} = \partial\Omega_{x_f}(x_s)$, of the interval $\Omega_{x_f}(x_s)$. In Eq. (11.9), $N_f^{(m\sigma)}(x_s) \equiv N_f^{(m\sigma)}$, $D_f^{(m\sigma)}(x_s) \equiv D_f^{(m\sigma)}$, unless specially declared, are determined by the relations $N_f^{(m\sigma)} = 1$, $D_f^{(m\sigma)} = 0$ at $m = 0$, $\sigma = +1$, (or at $\sigma = 0$, i.e., without parity separation), $N_f^{(m\sigma)} = 0$, $D_f^{(m\sigma)} = 1$ at $m = 0$, $\sigma = -1$ or at $m \neq 0$. The eigenfunctions satisfy the orthonormality condition in the same interval:

$$\langle i|j\rangle = \left\langle \Phi_i^{m\sigma}|\Phi_j^{m\sigma}\right\rangle = \int_{x_f^{\min}(x_s)}^{x_f^{\max}(x_s)} \Phi_i^{m\sigma}(x_f; x_s)\Phi_j^{m\sigma}(x_f; x_s)g_{1f}(x_f)dx_f = \delta_{ij}. \quad (11.10)$$

Here $\check{\lambda}_1(x_s) < \ldots < \check{\lambda}_{j_{\max}}(x_s) < \ldots$ is the desired set of real-valued eigenvalues. The corresponding set of potential curves of Eqs. (11.6) is determined by the condition $2E_j(x_s) = g_{3s}^{-1}(x_f; x_s)\check{\lambda}_j(x_s)$. The solutions of the problem (11.8)–(11.10) are calculated in the analytical form [18, 20], or by the program ODPEVP [12].

Substituting the expansion (11.7) into Eq. (11.4) in consideration of (11.8) and (11.10), we get a set of ODEs with respect to unknown $\chi^{(t)}(x_s) = (\emptyset_1^{(t)}(x_s), \ldots, \chi_{j_{\max}}^{(t)}(x_s))^T$

$$\sum_{j=1}^{j_{max}} \left\langle i|g_{1s}(x_f; x_s)[\hat{H}(x_f, x_s) - 2E_t]|j\right\rangle \chi_j^{(m\sigma t)}(x_s) = 0, \quad (11.11)$$

where the matrix elements read as

$$\left\langle i|g_{1s}(x_f; x_s)\hat{H}(x_f, x_s)|j\right\rangle = -\delta_{ij}\frac{d}{dx_s}g_{2s}(x_s)\frac{d}{dx_s} + <i|(\frac{g_{1s}(x_s)}{g_{3s}(x_s)}|j> \check{\lambda}_j(x_s)$$

$$+ <i|g_{1s}(x_s)\check{V}_s(x_s)|j> + g_{2s}(x_s)\left[W_{ij}(x_s) + Q_{ij}(x_s)\frac{d}{dx_s}\right] + \frac{dg_{2s}(x_s)Q_{ij}(x_s)}{dx_s}, \quad (11.12)$$

Here $W_{ij}(x_s)$, and $Q_{ij}(x_s)$, $\langle i|g_{1s}(x_s)|j\rangle$ and etc. are given by integrals

$$\langle i|g_{1s}(x_s)|j\rangle = \int_{x_f^{\min}(x_s)}^{x_f^{\max}(x_s)} g_{1f}(x_f)\Phi_i^{m\sigma}(x_f; x_s)g_{1s}(x_f; x_s)\Phi_j^{m\sigma}(x_f; x_s)dx_f, \quad (11.13)$$

$$W_{ij}(x_s) = W_{ji}(x_s) = \int_{x_f^{\min}(x_s)}^{x_f^{\max}(x_s)} g_{1f}(x_f)\frac{\partial\Phi_i^{m\sigma}(x_f; x_s)}{\partial x_s}\frac{\partial\Phi_j^{m\sigma}(x_f; x_s)}{\partial x_s}dx_f,$$

$$Q_{ij}(x_s) = -Q_{ji}(x_s) = -\int_{x_f^{\min}(x_s)}^{x_f^{\max}(x_s)} g_{1f}(x_f)\Phi_i^{m\sigma}(x_f; x_s)\frac{\partial\Phi_j^{m\sigma}(x_f; x_s)}{\partial x_s}dx_f,$$

calculated analytically [18, 20] or by using the program ODPEVP [12]. The solutions $\chi^{(m\sigma t)}(x_s) = \chi^{(t)}(x_s)$ of discrete spectrum $\mathcal{E} = 2E : 2E_1 < 2E_2 \leq \ldots \leq 2E_t \leq \ldots$ obey the BCs at points $x_s^t = \{x_s^{\min}, x_s^{\max}\} = \partial\Omega_{x_s}$ bounding the interval Ω_{x_s}:

$$\lim_{x_s \to x_s^t} \left(N_s^{(m\sigma)} g_{2s}(x_s) \frac{d\chi^{(m\sigma t)}(x_s)}{dx_s} + D_s^{(m\sigma)} \chi^{(m\sigma t)}(x_s) \right) = 0, \qquad (11.14)$$

where $N_s^{(m\sigma)} = 1$, $D_s^{(m\sigma)} = 0$ at $m = 0$, $\sigma = +1$, (or at $\sigma = 0$, i.e without parity separation), $N_s^{(m\sigma)} = 0$, $D_s^{(m\sigma)} = 1$ at $m = 0$, $\sigma = -1$ or at $m \neq 0$. They obey the orthonormality conditions (11.3) with $g_{1s}(x_f; x_s)$ from Table 11.1 and the KM expansion (11.7), that after integration (11.13) over x_f are reduced to

$$\left\langle \chi^{(m\sigma t)} | \chi^{(m\sigma t')} \right\rangle = \sum_{i,j=1}^{j_{max}} \int_{x_s^{\min}}^{x_s^{\max}} \chi_i^{(m\sigma t)}(x_s) \langle i | g_{1s}(x_s) | j \rangle \chi_j^{(m\sigma t')}(x_s) dx_s = \delta_{tt'}. \quad (11.15)$$

Solutions of BVP (11.11)–(11.15) are calculated with a given accuracy not vorse then six significant digits by the program KANTBP [9, 11].

Remark 1. Note t is the eigenvalue number in the ascending energy sequence $E_1 \leq E_2 \leq \ldots \leq E_t \leq \ldots$ corresponding to the number v of the eigenvalue $E_{t;j1} \leq E_{t;j2} \leq \ldots \leq E_{t;jv} \leq \ldots$ counted at each $\langle j \rangle = j$, in diagonal approximation of the KM Eqs. (11.11)–(11.12) or a crude AA Eq. (11.16) without diagonal nonadiabatic terms $W_{jj}(x_s)$, where number v determines the number $v-1$ of nodes of the solution $\chi_j^{(v)}(x_s)$ at fixed value j and the quantity $\langle j \rangle = \left\langle \chi^{(t)} | j | \chi^{(t)} \right\rangle$ is the averaged quantum number [10].

11.4 Numerical Calculations of the Energy Spectrum

After the separation of the angular variable φ, the axially symmetric BVP for the electron, hole, and exciton eigenstates in an impenetrable cone-shaped quantum dot (CQD) or spheroidal quantum dot (SQD) is reduced to the BVP (11.1)–(11.3) at $d = 2$ with respect to the radial $x_1 = \rho$ and the axial $x_2 = z$ variables, where $g_0(x) = \rho$, $g_{11}(x) = g_{22}(x) = \rho$, $g_{12}(x) = g_{21}(x) = 0$, $V(x) = V(\rho, z) = m^2/\rho^2 + 2V_C(\rho, z)$, with the BCs at the boundary $\partial\Omega = \partial\Omega_1 \cup \partial\Omega_2$, $\partial\Omega_1 = \{(\rho, z) | z = 0, \rho = \rho_{\max}(z)\}$, $\partial\Omega_2 = \{(\rho, z) | \rho = 0\}$ of the 2D domain $\Omega = \{(\rho, z) | \rho \geq 0, z \geq 0, \rho \leq \rho_{\max}(z)\}$

$$\Psi_t^{(m\sigma)}(\rho, z) | \partial\Omega_2 = 0, \quad \lim_{\rho \to 0} \left(\rho \frac{\Psi_t^{(m\sigma)}(\rho, z)}{\partial\rho} \delta_{m0} + \Psi_t^{(m\sigma)}(\rho, z)(1 - \delta_{m0}) \right) \bigg| \partial\Omega_1 = 0.$$

Below we restrict ourselves to the case $m = 0$. For CDQ $\rho_{\max}(z) = R(1 - z/H)$, where R is the base radius and H is the height, $\sigma = 0$, for SDQ, $\rho^2/a^2 + z^2/c^2 = 1$, where a and c are the spheroid semiaxes, and $\rho_{\max}(z) = a\sqrt{1 - z^2/c^2}$, $\sigma = +1$.

For oblate and prolate SDQs the BVP (11.1)–(11.3) at $d = 2$ was also solved in the spheroidal coordinates $(x_1 = \xi, x_2 = \eta)$, $g_0(x) = (f/2)^2(\xi^2 \pm \eta^2)$, $g_{11}(x) =$

Table 11.2 The first three eigenvalues, $\mathcal{E}_t(n_b, l_{\min})$, $t = 1, 2, 3$, at $m = 0$, $\sigma = +1$ in the units of E_R, for the oblate SQD $a = 2.5$, $c = 0.5$ obtained on the different FEM grid with the maximal element size $l_{\min}$. The number n_b determines the length of the polygonal boundary approximating the boundary of SQD. KM—Kantorovich method with 60 basis functions from [20]. SPH—FEM in spheroidal coordinates on non-uniform grid in the rectangular domain $0 < \xi_0 < c/\sqrt{a^2 - c^2} = 1/2\sqrt{6}$, $0 \le \eta \le 1$

$l_{\min}$	0.0625	0.125	0.03125	0.0625	KM	SPH
n_b	0.03125	0.03125	0.015625	0.015625		
$t = 1$	12.76518	12.76516	12.76490	12.76490	12.764809	12.77105
$t = 2$	20.04147	20.04143	20.04086	20.04085	20.040651	20.04933
$t = 3$	29.74910	29.74902	29.74780	29.74779	29.747387	29.75713

$(\xi^2 \pm 1)$, $g_{22}(x) = (1 - \eta^2)$, $g_{12}(x) = g_{21}(x) = 0$, $(f/2)^2 = \pm(a^2 - c^2)$, f is a focal distance, $V(x) = V(\xi, \eta) = m^2/(\xi^2 \pm 1)(1 - \eta^2)$, and using the Kantorovich method Eqs. (11.11)–(11.15) with $j_{max} = 60$ of basis functions [18].

The comparison of results obtained for eigenvalues of oblate SDQ in the cylindrical coordinates on different FEM grids, in the spheroidal coordinates, and using the (KM) is resented in Table 11.2 [1]. As seen from Table 11.2, the results coincide to five significant digits, and the maximal contribution to the error in cylindrical coordinates is due to the error of approximating the curved boundary by triangle finite elements with rectilinear boundaries.

Figures 11.1 and 11.2 show the lower part of non-equidistant spectrum $\tilde{E}(\zeta_{ca})/E_R = 2E_t$ (or $\tilde{E}(\zeta_{ac})/E_R = 2E_t$) and the eigenfunctions $\Psi_t^{m\sigma}$ from (11.7) for even states oblate (or prolate) SQD at $m = 0$.

For an oblate (or prolate) SQD a correspondence rule holds: $j = n_o = n_{zo} + 1 = 2n - (1 + \sigma)/2$, $n = 1, 2, \ldots, n_{\rho o} = (l - |m| - (1 - \sigma)/2)/2$ (or $j = n_{\rho p} + 1 = n_p = n = n_r + 1$, $j = 1, 2, \ldots, n_{zp} = l - |m|$) between the spherical quantum numbers $(n, l, m, \hat{\sigma})$ of an SQD with radius $r_0 = a = c$ and spheroidal quantum numbers $\{n_\xi = n_r, n_\eta = l - |m|, m, \sigma\}$ of an oblate (or prolate) SQD with the major semiaxis a (or c) and the minor semiaxis c (or a), and the adiabatic set of cylindrical quantum numbers $[n_{zo}, n_{\rho o}, m, \sigma]$ (or $[n_{\rho p}, n_{zp}, m, \sigma]$) upon continuous variation of parameter $\zeta_{ca} = c/a$ (or $\zeta_{ac} = a/c$).

The crossing of similar-parity energy levels in Figs. 11.1 and 11.2 upon the change of symmetry from spherical $\zeta_{ca} = 1$ ($\zeta_{ac} = 1$) to axial, i.e., upon the variation of the parameter $0 < \zeta_{ca} < 1$ ($0 < \zeta_{ac} < 1$), in the BVP with two variables at fixed m for an impenetrable oblate (prolate) SQDs is caused by the possibility to separate the variables $(\xi, \eta \, \varphi)$ and the additional integral of motion given explicitly [18] with

---

[1] For electron(e) and hole(h) states $2V_C(\rho, z) = 0$, and for exciton states $2V_C(\rho, z) = -2/\sqrt{\rho^2 + z^2}$, $2V_C(\rho, z) = \tilde{V}_C(\tilde{\rho}, \tilde{z})/E_R$, $\tilde{V}_C(\tilde{\rho}, \tilde{z}) = -2e/(\kappa\sqrt{\tilde{\rho}^2 + \tilde{z}^2})$, where e and m_e are the electron charge and mass, κ is the static permittivity. For GaAs model we use the reduced atomic units, $m_e^* = 0.067m_e$, $m_h^* = m_e^*/0.12$, $\kappa = 13.18$, $a_B = 104$Å, $E_R = 5.275$ meV, i.e., $\mathcal{E} = 2E = \tilde{E}/E_R$, $\Psi(\rho, z) = a_B^{3/2}\tilde{\Psi}^e(\tilde{\rho}, \tilde{z})$, $\rho = \tilde{\rho}/a_B$, $z = \tilde{z}/a_B$, where $\tilde{E}$, $\tilde{V}_C(\tilde{\rho}, \tilde{z})$, $\tilde{\rho}$ and $\tilde{z}$ are dimensioned quantities.
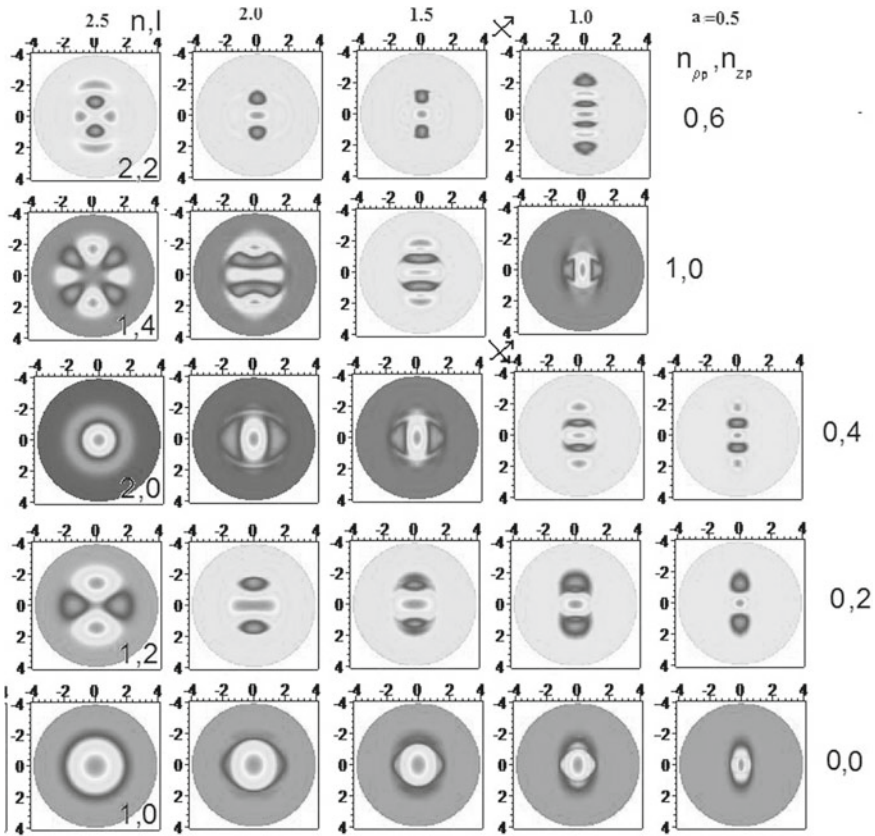
Fig. 11.2 Contour lines of the first five wave functions $\sigma = +1$, $m = 0$ in the xz plane of prolate SQD for the major semiaxis $c = 2.5$ and different values of the minor semiaxis a ($\zeta_{ac} = a/c \in (1/5, 1)$). Arrows show transformations of a shape of eigenfunctions passing thought exact crossing points of pairs of eigenvalues

eigenvalues of a separation parameter having branch points for complex values f of the focal distance or parameter $(f/2)\sqrt{2E}$ of the propagation constant [23, 24]. Thus, the values of parameter $0 < \zeta_{ca} < 1$, or $0 < \zeta_{ac} < 1$, corresponding to crossing points of the eigenvalues $\tilde{E}(\zeta_{ca})/E_R = 2E_t$, or $\tilde{E}(\zeta_{ac})/E_R = 2E_t$ of the lower parts of spectra of oblate or prolate SQDs, strongly restrict the range of applicability of the AA (in the strong size quantization limit), or diagonal approximation of the KM for their estimations.

11.5   Adiabatic Approximation and Size Quantization

For classification and approximate calculation of the spectrum under the size quantization (SQ) conditions for electron (e) hole (h) states the AA is used, $\Psi_{jv}^{m\sigma}(x_f, x_s) = \Phi_j^{m\sigma}(x_f; x_s)\chi_j^{(m\sigma v)}(x_s)$. For prolate SQD $a/c \ll 1$ and CQD with small apex angle $R/H \ll 1$, the parametric spectrum $2E_j^{m\sigma}(z)$ and eigenfunctions $\Phi_j^{(m\sigma)}(\rho; z)$ at $x_f = \rho, x_s = z$ of the 'fast' subsystem are solutions of BVP (11.8)–(11.10) at each value of parameter z that are expressed in terms of the cylindrical Bessel function of the first kind [20, 21]

$$2E_j^{m\sigma}(z) = \frac{\alpha_{n_{\rho\rho}+1,|m|}^2}{\rho_{\max}(z)^2}, \quad \Phi_j^{m\sigma=0}(\rho; z) = \frac{\sqrt{2}J_{|m|}(\rho\sqrt{2E_i(z)})}{\rho_{\max}(z)J_{|m+1|}(\alpha_{n_{\rho\rho}+1,|m|})},$$

where $\alpha_{n_{\rho\rho}+1,|m|}$ is the $j = n_p = n_{\rho\rho}+1$-th positive node of the Bessel function [22] $J_{|m|}(\rho_{\max}(z))$, $j = n_p = n_{\rho\rho}+1 = 1, 2, ...$

A low part of the spectrum $\mathcal{E}_{t;jv} = 2E_{t;jv}$, and eigenfunctions $\chi_j^{m\sigma v}(z)$ of the 'slow' subsystem are solutions of the BVP of the KM Eqs. (11.11)–(11.15) in diagonal approximation without diagonal nonadiabatic terms $W_{jj}(x_s)$, i.e. in a crude AA, where number $v = n_{zp}+1$ determines the number $v-1 = n_{zp}$ of nodes of the solutions $\chi_j^{(m\sigma v)}(z)$ at fixed j:

$$(-\frac{\partial^2}{\partial z^2} + 2E_j^{m\sigma}(z) - \mathcal{E}_{t;jv})\chi_j^{(m\sigma v)}(z) = 0, \tag{11.16}$$

that are subjected to orthogonal and normalization conditions

$$\int\limits_{z^{\min}}^{z^{\max}} dz\chi_j^{m\sigma v}(z)\chi_j^{m\sigma v'}(z) = \delta_{vv'} \tag{11.17}$$

with the BCs $\chi_j^{m\sigma v}(0) = \chi_j^{m\sigma v}(H) = 0$ at $\sigma = 0$ for CQD, or $\chi_j^{m\sigma v}(-c) = \chi_j^{m\sigma v}(c) = 0$ at $\sigma = \pm 1$ for SQD. Considering (11.16), (11.17) in the linear or quadratic approximation for the prolate CQD or SQD leads to the spectrum in the analytical form [20, 21]

$$\mathcal{E}_{(t;n_p n_{zp} m)}^{CQD} = 2E_{n_p m}^{(0)} + 2\varepsilon_{n_{zp}} = \frac{2\alpha_{n_p,|m|}^2}{R^2} - \left(\frac{2\alpha_{n_p,|m|}^2}{R^2 H}\right)^{2/3}\beta_{n_{zp}+1},$$

$$\mathcal{E}_{(t;n_p n_{zp} m)}^{PSQD} = \frac{\alpha_{n_p,|m|}^2}{a^2} + \frac{\alpha_{n_p,|m|}^2}{ac}(2n_{zp} + 1),$$

where $\beta_{n_{zp}+1}$ is the v-th negative node of the Airy function of the first kind [22]. For oblate SQD $c/a \ll 1$ and CQD $H/R \ll 1$, using the AA at $x_f = z, x_s = \rho$, one has the spectrum and eigenfunctions classified by set $[n_{zo}, n_{\rho o}, m, \sigma]$.

Table 11.3 Comparison of the Coulomb interaction energy $\mathcal{E}_t^{eh}$ between electron and hole, and the size quantization energy $\mathcal{E}_t^{SQ}$ in the units of E_R. Here $H = 10a_B$, $m = 0$. The corresponding values of $\mathcal{E}_{(t;n_p n_{zp} m)}^{SQ}$ (adiabatic calculation) and $\mathcal{E}_{(t;n_p n_{zp} m)}^{eh}$ (first-order perturbation theory) adopted from Ref. [21] are labeled by an asterisk *

R (a_B)	$(t; n_{\rho p}, n_{zp}) = (1; 0, 0)$		$(t; n_{\rho p}, n_{zp}) = (18; 1, 0)$		$(t; n_{\rho p}, n_{zp}) = (2; 0, 1)$	
	$\mathcal{E}_t^{SQ}$	$\mathcal{E}_t^{eh}$	$\mathcal{E}_t^{SQ}$	$\mathcal{E}_t^{eh}$	$\mathcal{E}_t^{SQ}$	$\mathcal{E}_t^{eh}$
0.5	30.42114	−2.64009	142.96526	−4.19801	36.95117	−1.88114
0.5	26.624*	−1.121*	141.542*	−1.113*	34.483*	−0.95*
1.0	8.88906	−1.71413	39.22966	−2.27799	11.93808	−1.25028
1.0	8.359*	−0.902*	36.272*	−1.021*	10.287*	−0.608*
1.5	4.49383	−1.33844	18.79476	−1.66173	6.51718	−0.99660
1.5	4.071*	−0.781*	18.085*	−0.762*	5.193*	−0.503*

Table 11.3 presents the comparison of the energy of Coulomb interaction of exciton $\mathcal{E}_t^{eh} = \mathcal{E}_t^C m_h^*/(m_e^* + m_h^*) - \mathcal{E}_t^{SQ}$ with the size quantization electron energy $\mathcal{E}_t^{SQ}$ at different geometric parameters of a CQD, where exciton energy $\mathcal{E}_t^C$ with the electron-hole reduced mass $m_{eh} = m_e^* m_h^*/(m_e^* + m_h^*)$ in the exciton center-of-mass frame and size quantization electron energy $\mathcal{E}_t^{SQ}$ with the electron mass m_e^* were obtained by solving the BVP (11.1)–(11.3) with Coulomb potential $2V_C(\rho, z)$ and without it, correspondingly. From Table 11.3 the correction energy $\mathcal{E}_t^{eh}$ is always seen to be negative, and with the increasing radius R the relative contribution of Coulomb energy of exciton becomes significant. The comparison with $\mathcal{E}_{(t;n_p n_{zp} m)}^{SQ}$ and $\mathcal{E}_{(t;n_p n_{zp} m)}^{eh}$ calculated using the AA and the perturbation theory [21] show the contribution of nonadiabatic corrections and the applicability of the AA.

Figure 11.3 shows the dependence of the charge carrier energies upon the base radius of fixed-height CQDs and the minor semiaxis of fixed-major semiaxes SQDs, and upon the apex angle of fixed-volume CQDs and SQDs, respectively. Note that each eigenlevel of the 'fast' subsystem has a family of 'slow' subsystem eigenlevels positioned thereupon. For example, for CQD with $\tilde{R} = 0.5a_B$, $\tilde{H} = 10a_B$, the first level $((t, n_\rho, n_z) = (1, 0, 0)$, $\tilde{E}_1^{SQ}/E_R = 30.42114)$ and the eighteenth $((t, n_\rho, n_z) = (18, 1, 0)$, $\tilde{E}_{18}^{SQ}/E_R = 142.96526$) one belong to the 'fast' subsystem levels. For $\tilde{R} = 1.5a_B$ the first level and the seventh one belong to the 'fast' subsystem, while five levels between them belong to the 'slow' subsystem, etc. The carrier energy is seen to decrease with the increasing base radius $\tilde{R}$ or small semiaxis $\tilde{a}$, because the SQ contribution to the energy decreases. The crossing of the seventh level with the eighth one at $\tilde{R} \approx 1.5a_B$ corresponds to the crossing of the same levels at $\theta_0 \approx \arctan(3/20)$.

Figure 11.3a and b show that for prolate CQD and SDQ the faster growth of energy at small apex angles θ_0 is caused by the size quantization in radial variable ρ and angular variable φ. The slower increase in energy at the apex angles approaching the right angle is caused by the size quantization in longitudinal variable z, i.e., the height. The difference in the rate of energy level variation in the adiabatic domains of variation of geometric parameters is due to the nonuniform scale, since the radius
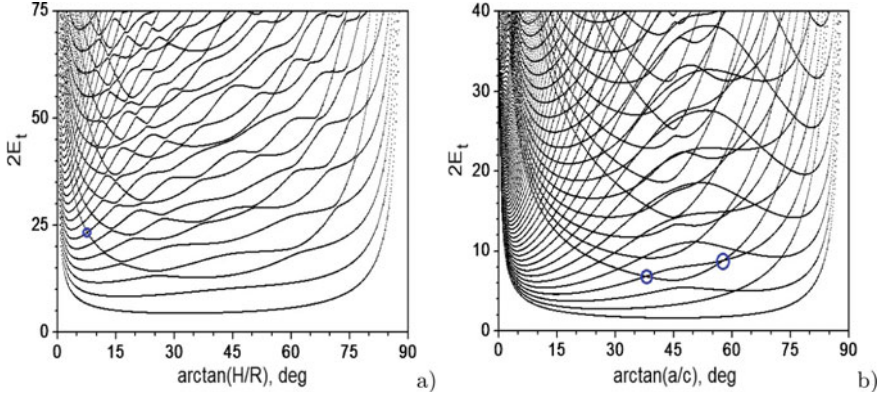
Fig. 11.3 Energy levels $\mathcal{E}_t = 2E_t = \tilde{E}_t^{SQ}/E_R$ at $m = 0$: **a** for prolate and oblate CQDs of equal volume $V = \pi R^2 H/3 = (15/2)\pi a_B^3$ at the base of $H = 10$ and $R = 1.5$ versus the stretch angle $\theta_0 = \arctan(H/R)$ at the base of $\theta_0 \approx 8.53°$, and **b** for prolate and oblate SQDs of equal volume $V = 4\pi a^2 c/3 = (125/6)\pi a_B^3$ at the base of $a = c = 2.5$ versus $\theta_0 = \arctan(a/c)$ at the base of $\theta_0 = 45°$

varies as $(\tan\theta_0)^{2/3}$ and the height as $(\cot\theta_0)^{1/3}$. It is also seen that for the angle values beyond the adiabatic domains there are series of quasicrossings and exact crossings of energy levels for CQD (for comparison, see a discussion of crossing points in the spectra of triangles [25–27]) and SQD, respectively, and its transformation to the oblate QDs.

Remark 2. The above analysis shows the following: the small values of parameters $0 < \zeta_{ca} < 1$ and $H/R \ll 1$, or $0 < \zeta_{ac} < 1$ and $R/H \ll 1$, corresponding to exact crossing and quasicrossings points of eigenvalues in the lower part of the energy spectrum of oblate or prolate QDs strongly restrict the applicability range of the adiabatic approximation (in the strong size quantization limit), or diagonal approximation of Kantorovich method for their estimations.

11.6 Interband Absorption

Consider the direct interband absorption in cone-shaped quantum dots in the regime of strong size quantization, when the Coulomb interaction between an electron and a hole can be neglected. Furthermore, consider the case of a heavy hole with $m_e^* \ll m_h^*$, where m_e^* and m_h^* are the electron and hole effective mass, respectively. Then the absorption coefficient is given by [28]

$$\tilde{K}(\tilde{\omega}^{ph}) = \sum_{\nu\nu'} \tilde{K}_{\nu\nu'}(\tilde{\omega}^{ph}) = \tilde{K}_0 \sum_{\nu\nu'} \left| \int \tilde{\Psi}_\nu^e \tilde{\Psi}_{\nu'}^h d\mathbf{r} \right|^2 \delta(\hbar\tilde{\omega}^{ph} - \tilde{E}_g - \tilde{E}_\nu^e - \tilde{E}_{\nu'}^h),$$
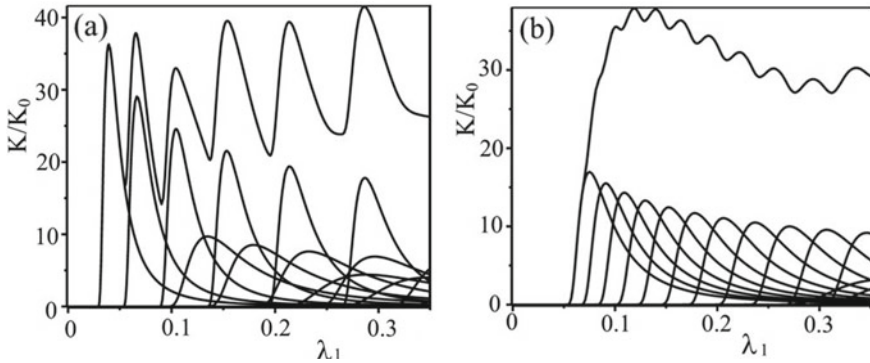
$$(11.18)$$

where $\tilde{\Psi}^{e(h)}_{\nu(\nu')}$ are envelopes of the electron and hole wave functions, $\nu = [n_{\rho p}n_{zp}m]$ and $\nu' = [n'_{\rho p}n'_{zp}m']$ ($\nu = [n_{zo}n_{\rho o}m]$ and $\nu' = [n'_{zo}n'_{\rho o}m']$) are sets of quantum numbers corresponding to the electron and the heavy hole prolate(oblate) SQD or CQD, respectively, $\tilde{E}_g$ is the band gap of the bulk semiconductor (for GaAs $\tilde{E}_g/E_R = 1.43/(5.27 \cdot 10^{-3})$), $\tilde{\omega}^{ph}$ is the frequency of the incident light, and $\tilde{K}_0$ is proportional to the square of the transition matrix element calculated with Bloch functions [28]. Here the following selection rules for the transitions between the levels with different quantum numbers are valid in the adiabatic classification. In the case of the prolate(oblate) SQD and CQD for the magnetic quantum number the transitions between the levels with $m = -m'$ are allowed. For the prolate(oblate) SQD the transitions between the levels with $n_{\rho p} = n'_{\rho p}$ and $n_{zp} = n'_{zp}$ ($n_{zo} = n'_{zo}$ and $n_{\rho o} = n'_{\rho o}$), respectively, are allowed. For the prolate(oblate)CQD transitions between the levels with $n_{\rho p} = n'_{\rho p}$ ($n_{zp} = n'_{zp}$) are allowed, however there is no selection rule for the axial(radial) quantum numbers n_{zp} ($n_{\rho o}$) and any transitions between different levels are allowed: $n_{zp} \rightarrow \forall n'_{zp}$ ($n_{\rho o} \rightarrow \forall n_{\rho o}$) respectively, like for prolate (oblate) SQD in uniform electric field [20].

The difference between energy levels for CQD of the same family increases with the increase in the axial quantum number. For example, $\Delta\tilde{E}_{10} = 1.1E_R$, when $\tilde{R} = 1.5a_B$ and $\tilde{H} = 10a_B$ ($n_{\rho p} = 0, m = 0$), and $\Delta\tilde{E}_{10} = 3.4E_R$, when $\tilde{R} = 1.5a_B$ and $\tilde{H} = 10a_B$ ($n_{\rho p} = 1, m = 0$). Note that the transition frequency between these energy levels is $\Delta\tilde{\omega}^{ph}_{10}(n_{\rho p} = 0, m = 0) = 1.43 \cdot 10^{12}\text{sec}^{-1}$ and $\Delta\tilde{\omega}^{ph}_{10}(n_{\rho p} = 1, m = 0) = 4.3 \cdot 10^{12}\text{sec}^{-1}$, which falls into the IR range of spectrum.

In CQD the decrease in the base radius increases the absorption edge energy. It is due to the fact that with the decrease in $\tilde{R}$ the effective width of the bandgap increases due to smaller influence of the CQD walls. The energy levels corresponding to high values of the cone height are located above. Note that the interband transition frequency between the energy levels is $\tilde{\omega}^{ph}_{000} = 5.07 \cdot 10^{-14}\text{sec}^{-1}$ for $\tilde{R} = 0.2a_B$ and $\tilde{H} = 15a_B$, which falls into the visible spectral range [21].

For the Lifshits-Slezov distribution, Fig. 11.4 displays the total absorption coefficient $\tilde{K}(\tilde{\omega}^{ph})/\tilde{K}_0$ and the partial absorption coefficients $\tilde{K}_{\nu,\nu}(\tilde{\omega}^{ph})/\tilde{K}_0$, that form the corresponding partial sum (11.18) over a fixed set of quantum numbers ν, ν' at $m = -m' = 0$. In the regime of strong dimensional quantization, the frequencies of the interband transitions ($h \rightarrow e$) in GaAS between the levels $n_o = n_{zo}+1 = 1$, $n_{\rho o} = 0, m = 0$ for oblate SQD or $n_p = n_{\rho o}+1 = 1$, $n_{zp} = 0, m = 0$ for prolate SQD at the fixed values $\tilde{a} = 2.5a_e$ and $\tilde{c} = 0.5a_e$ for oblate SQD or $\tilde{a} = 0.5a_e$ and $\tilde{c} = 2.5a_e$ for prolate SQD, are equal to $\Delta\tilde{\omega}^{ph}_{100}/(2\pi) = 16.9$ THz or $\Delta\tilde{\omega}^{ph}_{100}/(2\pi) = 33.3$ THz, where $\Delta\tilde{\omega}^{ph}_{100}/(2\pi) = (\tilde{W}_{100,100}-\tilde{E}_g)/(2\pi\hbar)$, $\tilde{W}_{\nu,\nu'} = \tilde{E}_g+\tilde{E}^e_\nu+\tilde{E}^h_{\nu'}$ correspond to the IR spectral region, taking the band gap value $(2\pi\hbar)^{-1}\tilde{E}_g = 346$ THz [20].

With the decreasing semiaxis the threshold energy increases, because the 'effective' band gap width increases, which is a consequence of the dimensional quantization enhancement. Therefore, the above frequency is greater for prolate QD than for oblate QD, because the QD implemented in two directions of the plane (x,y) is effectively larger than that in the direction of the z axis solely at similar values of semiaxes. Higher-accuracy calculations reveal essential difference in the frequency

Fig. 11.4 Absorption coefficient K/K_0, Eq. (11.18), consisting of a sum of the first partial contributions versus the energy $\lambda = \lambda_1 = (\tilde{\omega}^{ph} - \tilde{E}_g)/\tilde{E}_g$ of the optical interband transitions for ensembles of GaAs SQDs ($h \rightarrow e$) with the Lifshits-Slezov distribution of the random small semiaxis for an ensemble of **a** oblate SQDs $\bar{c} = 0.5$, $a = 2.5$ and **b** prolate SQDs $\bar{a} = 0.5$, $c = 2.5$

behavior of the AC for interband transitions in the systems of semiconductor oblate or prolate QDs having a distribution of minor semiaxes, which can be used to verify the above models.

11.7 Conclusion

In this paper we briefly review the efficient methods and software for calculating electron, hole and exciton states in axially symmetric QDs by the example of cone-shaped and spheroidal impenetrable QDs. Our analysis shows that the calculation schemes of high-order FEM implemented on unstructured grids together with complementary KM and AA (in the strong size quantization limit) provide useful numerical and analytical tools for describing the energy spectra and *their crossing points that determine the range of AA applicability*, and the optical absorption coefficient in an ensemble of non-interacting axially symmetric QDs.

Further development and application of such approach and software is associated with the investigation of spectral and optical characteristics of quantum wells, wires and dots with complex geometry.

References

1. Harrison, P.: Quantum Wells. Wires and Dots. Theoretical and Computational Physics of Semiconductor Nanostructures. Wiley, New York (2005)
2. Ciarlet, P.: The Finite Element Method for Elliptic Problems. North-Holland Publ. Comp, Amsterdam (1978)

3. Ramdas Ram-Mohan, L.: Finite Element and Boundary Element Applications in Quantum Mechanics. Oxford Univ. Press, New York (2002)

4. Gusev, A. A., Gerdt, V. P., Chuluunbaatar, O., Chuluunbaatar, G. , Vinitsky, S.I., Derbov, V.L., Gozdz, A.: Symbolic-numerical algorithms for solving the parametric self-adjoint 2D elliptic boundary-value problem using high-accuracy finite element method. V.P. Gerdt et al. (Eds.): CASC 2017, LNCS **10490**, 151-166 (2017)

5. Gusev, A. A., Gerdt, V. P., Chuluunbaatar, O., Chuluunbaatar, G. , Vinitsky, S.I., Derbov, V.L., Gozdz, A.: Symbolic-numerical algorithm for generating interpolation multivariate hermite polynomials of high-accuracy finite element method. V.P. Gerdt et al. (Eds.): CASC 2017, LNCS **10490**, 134-150 (2017)

6. Gusev, A.A., Chuluunbaatar, O., Vinitsky, S.I., Derbov, V.L., Hai, L.L., Kazaryan, E.M., Sarkisyan, H.A.: Finite element method for calculating spectral and optical characteristics of axially symmetric quantum dots. SPIE **10717**, 1071712 (2018)

7. Vinasco, J.A., Radu, A., Tiutiunnyk, A., Restrepo, R.L., Laroze, D., Feddi, E., Mora-Ramos, M.E., Morales, A.L., Duque, C.A.: Revisiting the adiabatic approximation for bound states calculation in axisymmetric and asymmetrical quantum structures. Superlattices and Microstructures **138**, 106384 (2020)

8. Kantorovich, L.V., Krylov, V.I.: Approximate Methods of Higher Analysis. Wiley, New York (1964)

9. Chuluunbaatar, O., Gusev, A.A., Gerdt, V.P., Rostovtsev, V.A., Vinitsky, S.I., Abrashkevich, A.G., Kaschiev, M.S., Serov, V.V.: POTHMF: A program for computing potential curves and matrix elements of the coupled adiabatic radial equations for a hydrogen-like atom in a homogeneous magnetic field. Comput. Phys. Commun. **178**, 301–330 (2008)

10. Gusev, A., Vinitsky,S. Chuluunbaatar, O., Gerdt, V., Hai, L. L., Rostovtsev, V.: Symbolic-Numerical Calculations of High-$|m|$ Rydberg States and Decay Rates in Strong Magnetic Fields. V.P. Gerdt et al. (Eds.): CASC 2012, LNCS **7442**, 155-171, (2012)

11. Chuluunbaatar, O., Gusev, A.A., Vinitsky, S.I. and Abrashkevich, A.G.: KANTBP 2.0: New version of a program for computing energy levels, reaction matrix and radial wave functions in the coupled-channel hyperspherical adiabatic approach. Comput. Phys. Commun. **179**, 685–693 (2008)

12. Chuluunbaatar, O., Gusev, A.A., Vinitsky, S.I., Abrashkevich, A.G.: ODPEVP: A program for computing eigenvalues and eigenfunctions and their first derivatives with respect to the parameter of the parametric self-adjoined Sturm-Liouville problem. Comput. Phys. Commun. **181**, 1358–1375 (2009)

13. Derbov V.L., Serov V.V., Vinitsky S.I., Gusev A.A., Chuluunbaatar O., Kazaryan E.M., Sarkisyan A.A.: On Solving the Low-Dimensional Boundary Value Problems of Quantum Mechanics by Kantorovich Method - Reduction to Ordinary Differential Equations. Izvestiya of Saratov University. Physics: Izv. Saratov Univ. (N. S.), Ser. Physics, **10**, iss.1, 4–17 (2010), https://fizika.sgu.ru/en/node/239

14. Vinitsky,S., Gusev, A.A., Chuluunbaatar, O., Derbov,V.L., Zotkina, A.S.: On calculations of two-electron atoms in spheroidal coordinates mapping on hypersphere Proc. of SPIE **9917**, 99172Z (2016). https://doi.org/10.1117/12.2229528

15. Migdal, A.B.: Qualitative Methods in Quantum Theory (A.J. Leggett, Ed.) (1st ed.). CRC Press (1977)

16. Gusev, A.A., Chuluunbaatar, O., Vinitsky, S.I., Kazaryan, E.M., Sarkisyan, H.A.: The application of adiabatic method for the description of impurity states in quantum nanostructures. Journal of Physics: Conference Series **248**, 012047 (2010)

17. Gusev, A.A., Chuluunbaatar, O., Vinitsky, S.I., Derbov, V.L., Kazaryan, E.M., Kostanyan, A.A., Sarkisyan, H.A.: Adiabatic approach to the problem of a quantum well with a hydrogen - like impurity. Phys. Atom. Nucl. **73**, 331–338 (2010)

18. Gusev, A.A., Chuluunbaatar, O., Vinitsky, S.I., Dvoyan, K.G., Kazaryan, E.M., Sarkisyan, H.A., Derbov, V.L., Klombotskaya, A.S., Serov, V.V.: Adiabatic description of nonspherical quantum dot models. Phys. Atom. Nucl. **75**, 1210–1226 (2012)

19. Gusev, A.A., Chuluunbaatar, O., Hai, L,L., Vinitsky, S.I., Kazaryan, E.M., Sarkisyan, H.A., Derbov, V.L.: Spectral and optical characteristics of spheroidal quantum dots. Journal of Physics: Conference Series **393**, 012011 (2012)
20. Gusev, A.A., Hai, L.L., Vinitsky, S.I., Chuluunbaatar, O., Derbov, V.L., Klombotskaya, A.S., Dvoyan, K.G., Sarkisyan, H.A.: Analytical and numerical calculations of spectral and optical characteristics of spheroidal quantum dots. Phys. Atom. Nucl. **76**, 1033–1055 (2013)
21. Hayrapetyan, D.B., Chalyan, A.V., Kazaryan, E.M., Sarkisyan, H.A.: Direct interband light absorption in conical quantum dot. J. Nanomaterials **2015**, 915742 (2015)
22. Abramowitz, M., Stegun, I.A.: Handbook of Mathematical Functions. Dover, New York (1965)
23. Oguchi, T.: Eigenvalues of spheroidal wave functions and their branch points for complex values of propagation constant. Radio Sci. **5**(8–9), 1207–1214 (1970)
24. Skorokhodov, S.L., Khristoforov, D.V.: Calculation of the branch points of the eigenfunctions corresponding to wave spheroidal functions. Comput. Math. Math. Phys. **46**(7), 1132–1146 (2006)
25. Berry, M.V. and Wilkinson, M: Diabolical points in the spectra of triangles. Proc.R. Soc. Lond. A **392**, 15–43 (1984)
26. Pockels, F.: Über die Partielle Differential-Gleichung $\Delta u + k^2 u = 0$ und deren Auftreten in der Mathematischen Physik. B.G. Teubner, Leipzig (1891)
27. McCartin, B.J.: Laplacian Eigenstructure of the Equilateral Triangle. Hikari Ltd., Ruse, Bulgaria (2011)
28. Anselm, A.: Introduction to Semiconductor Theory. Mir, Moscow (1982).in Russian